Simulation of Fluid Flow inside a Continuous Slab-Casting Machine

B.G. THOMAS, L.J. MIKA, and F.M. NAJJAR

A finite element model has been developed and applied to compute the fluid flow distribution inside the shell in the mold region of a continuous, steel slab-casting machine. The model was produced with the commercial program FIDAP, which allows this nonlinear, highly turbulent problem to be simulated using the K-ε turbulence model. It consists of separate two-dimensional (2-D) models of the nozzle and a section through the mold, facing the broad face. The predicted flow patterns and velocity fields show reasonable agreement with experimental observations and measurements conducted using a transparent plastic water model. The effects of nozzle angle, casting speed, mold width, and turbulence simulation parameters on the flow pattern have been investigated. The overall flow field is relatively insensitive to process parameters.

I. INTRODUCTION

THE velocity distribution of molten steel contained within the solidifying shell of a continuous casting machine is very influential on the distribution of inclusion particles, which is important to the internal cleanliness and quality of the steel. In addition, the flow pattern has a great influence on heat transfer to the shell during the critical initial stages of solidification. To further understand this behavior, a 2-D finite element model has been developed to calculate the flow of molten steel within the liquid pool inside the shell in the mold region of a continuous slab-casting machine, fed by a bifurcated, submerged entry nozzle.

The first objective of this project was to develop a mathematical model of the flow pattern in the liquid pool which determines how both molten steel and inclusion particles carried in by the nozzle are distributed. To verify acceptable accuracy of the model, its predictions were compared with experiments conducted using a transparent plastic water model of the system.

The second objective was to investigate the effects of important casting operation and design variables on the fluid flow pattern. Of particular interest was the angle of the jet streaming in from the submerged nozzle, its approximate impingement point on the solidifying shell along the narrow face wall, and velocities down the wall. These parameters are important because of their influence on heat transfer and the growth of the solidifying shell.

This work represents the first step in the development of a comprehensive system of mathematical models of fluid flow, heat transfer, shrinkage, and stress generation within the continuous slab-casting mold, which will ultimately be applied to predict and understand the effects of such diverse variables as nozzle design and mold taper on defect generation in the solidifying shell. The results of the flow calculations described here are input to a separate heat flow model to calculate the temperature field within the molten steel and the resulting heat flux to the solidifying shell on the narrow face mold wall.

The superheat in the fluid steel can be convected to the shell and conducted through the shell to the copper mold walls, or it can be swept out of the mold region to be dissipated much lower in the caster. In addition, uneven dissipation of superheat to the shell will produce a maximum heat input near the point of jet impingement. This can produce local "hot spot(s)" on the shell, where growth is slow, and may cause shell thinning, erosion, and even lead to breakouts, particularly at higher casting speeds.[1]

Equally important is the influence of the flow pattern on the temperature of the steel at the narrow face near the meniscus. If the steel temperature is too low during the critical solidification stage, it is believed to exacerbate defect formation.[2] The results of this work should increase our understanding of the early stages of shell solidification in the mold and eventually provide insights that will aid in the prevention of breakouts and other quality problems, such as longitudinal cracks.

II. PREVIOUS WORK

Previous studies of the continuous slab-casting mold have mainly involved the use of full-scale water models.[2–5] These studies have revealed a great deal about the flow pattern, which has been confirmed with experience with operating steel casters. However, it is difficult to use the physical models to study the accompanying heat flow, which is more easily done using a mathematical model.

Although several mathematical models of fluid flow have recently been applied to many different steel processing operations (including ladles,[6] tundishes,[7,8] and nozzles[9]), only a few recent studies have been conducted to model fluid flow within a continuous-casting mold.[10,11] None of these studies have explored in much depth the effects of caster process variables on the flow pattern.

B.G. THOMAS, Assistant Professor, and F.M. NAJJAR, Graduate Student, are with the Department of Mechanical and Industrial Engineering, University of Illinois, Urbana, IL 61801. L.J. MIKA, formerly Graduate Student, Department of Mechanical and Industrial Engineering, University of Illinois–Urbana, is Research Engineer with Amoco Technology Company, Naperville, IL 60566.

Manuscript submitted November 3, 1988.

III. MODEL DESCRIPTION

A finite element model has been developed to simulate fluid flow in the mold region of a continuous slab caster, illustrated schematically in Figure 1. A 2-D vertical section parallel to the wide face through the center of the caster was chosen because the bifurcated nozzles used in slab casters, combined with the high aspect ratio of the slab mold, produce flow patterns whose major characteristics are exhibited in these two dimensions. Various lengths of a 1.32-m (52-inch)-wide slab caster were simulated, exploiting symmetry about the center line. The left side of the model domain is the center line of the caster. The right side is the inside of the "narrow face" of the solidifying steel shell, which is adjacent to the mold for the top 0.600 m. Fluid enters the model domain through an inlet surface which represents a nozzle port whose center is submerged 0.265 m below the meniscus and 0.365 m below the top of the 0.700-m-long mold.

The flow is highly turbulent, even far away from the nozzle, as indicated by the calculated Reynolds number of 12,000 at the mold exit (which is based on the data in Table I and treating the rectangular mold as an equivalent diameter pipe). Therefore, turbulence was incorporated into the present model. Due to the small time and length scales of the turbulence, it is only practical to solve for the time-averaged values of velocity. Thus, the two-equation K-ε model, which has been used previously to simulate a variety of turbulent flows,[6–9,12,13] was chosen to simulate the turbulent, recirculating flow involved in the present problem. The continuity, momentum, and turbulence equations which describe this problem are given in Appendix I. Further details can be found in the FIDAP manual[14] and elsewhere.[15] Single-phase flow was also assumed, so effects such as buoyancy from argon gas bubble injection were not considered in this study.

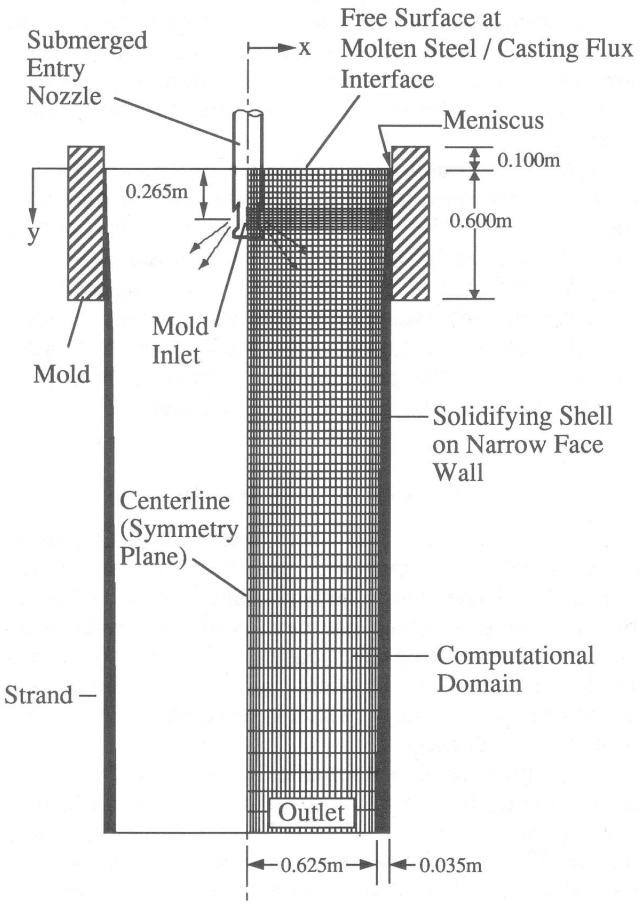

Fig. 1—Schematic of fluid flow and shell growth in a continuous slab caster showing simulation domain and mesh relative to the 700-mm-long mold.

A. *Boundary Conditions*

1. *Narrow face wall*

The flow was modeled up to, but not including, the mushy zone forming the inside of the steel shell solidifying against the narrow face mold wall. To account for buildup of the solid shell against the mold wall, the narrow face computational boundary can be tapered inward with distance down the mold wall. As expected, the model results were insensitive to the exact value of this small change in the size of the domain.

Most model runs employed a set of velocity boundary conditions at the wall known as "wall functions." These equations take into account that property variations are very large near the wall that forms the inside of the solidifying shell, and that the K-ε model turbulence equations are no longer valid in this region. Thus, the computational domain is ended at the edge of the laminar boundary layer found near the narrow face wall. Along this boundary, the velocity normal to the wall, v_x, is set to zero. In addition, boundary condition values are imposed on the tangential velocity gradient ($\partial v_y/\partial x$), K, and ε parameters, which are calculated using empirical equations or "wall functions." Further details regarding the wall functions can be found in Appendix I and elsewhere.[14,16]

2. *Inlet*

To derive the inlet velocity boundary conditions to the mold at the nozzle ports, a mass balance was performed in two dimensions, setting (nozzle port length * nozzle outlet velocity) equal to (mold domain outlet width * casting speed). An eight-node, parabolic input velocity profile was employed both to satisfy this constraint and to achieve the same average and peak velocities into the mold as found through the actual casting nozzle port. In order to achieve this, the nozzle port length had to be adjusted using the above mass balance equation.

Components of the nozzle port velocity and values for K and ε were fixed across the inlet boundary surface of the model. The accuracy of this method hinges on finding reasonable values for the velocities, K, and ε at the inlet. These values were therefore calculated using a separate fluid flow model of the nozzle itself, which is discussed later.

3. *Bottom outlet*

Except when simulating the plastic bottom of the physical model, normal gradients of all variables (including velocity, K, and ε) were left at zero along the bottom outlet surface of the computational model domain. Constraining the outlet flow in any other way, such as fixing the outlet vertical velocity to the casting speed, was found to produce unrealistic results.

Table I. Standard Input Conditions for Model Runs

Material	Steel	Water
Viscosity, μ	0.0055 Ns/m^2	0.000959 Ns/m^2
Density, ρ	7015 kg/m^3	1000 kg/m^3
Nominal nozzle angle	15 deg downward	15 deg downward
Number of nodes across inlet	8	4
Inlet jet width	0.0148 m	0.0432 m
Inlet and initial K (kinetic energy)	0.0502 m^2/s^2	0.0574 m^2/s^2
Inlet and initial ε (dissipation)	0.3935 m^2/s^3	0.4414 m^2/s^3
Boundary conditions at wall	wall functions	wall functions
Thickness of laminar boundary, y_n	0.01 m	0.01 m
Outlet boundary condition	zero gradients	zero normal velocity every 2nd node
Mesh size	32 × 73 elements	30 × 54 elements
Casting speed	0.0167 m/s	0.0167 m/s (1 m/min)
Half caster width simulated	0.660 m (52 in. mold)	0.6856 m (54 in. mold)
Caster length simulated	3.00 m	1.118 m
Nozzle submergence depth	0.265 m	0.265 m

4. *Top surface and center line*

Along the center line symmetry plane (the left side) and the top face of the model (the steel-casting powder interface), the normal velocities were constrained to zero. Observations of casters and water models indicate that the surface is relatively quiescent, so no free surface representation was required or attempted.

B. *Solution Methodology*

The commercial finite element program FIDAP was chosen to model this complex problem, because it is capable of simulating three dimensional (3-D) turbulent fluid flow coupled with heat transfer. The standard mesh, shown in Figure 1, consists of a 32 by 73 grid of four-node, linear, quadrilateral elements and 73 two-node linear wall elements along the right side boundary. A refined 40 by 75 mesh was used for later runs. Both meshes are graded with smaller elements found near the walls and inlet area. The current solution strategy consists of four successive substitutions (using proper fluid properties), followed by reforming the stiffness matrix, then performing further successive substitutions using an under-relaxation factor of 0.5 or 0.6, until the relative error in the residual force vector is stably reduced to less than 1 pct. This method usually produces convergence in about 20 iterations total and requires about 8 hours of execution time on a Ridge 32S computer or 7 CPU minutes on a CRAY X/MP.* Experience is required to control the solution procedure to achieve convergence for each given simulation, and further details regarding the strategies are given elsewhere.[14,16]

*CRAY X/MP is a trademark of Cray Research Inc., Minneapolis, MN.

IV. NOZZLE MODEL

The angle of the fluid leaving the submerged inlet nozzle is known to have a great influence on both fluid flow in the mold and heat transfer to the growing shell.[1] Observations of the physical water model at Inland Steel, East Chicago, IN, revealed that the flow leaves the nozzle at a steeper downward angle than the nominal angle built into the nozzle exit ports. In addition, the velocity distribution over the nozzle outlet is skewed, with most of the fluid leaving the lower half of the nozzle port openings and some recirculating fluid actually entering the upper part. To determine the proper boundary conditions for the inlet of the caster model (inlet angle, K, and ε), a separate model for fluid flow within this nozzle was developed.

A. *Nozzle Model Formulation*

The model currently is based on a bifurcated nozzle used by Inland Steel with outlet ports angled 15 deg down from the horizontal. The domain employed for simulation of the nozzle flow exploits symmetry by modeling half of a vertical cross section through the nozzle. Since the width of the square 65 by 90-mm outlet ports is almost equal to the bore of the nozzle (76 mm), the 2-D approximation seems reasonable. The normal (vertical) velocity into the nozzle inlet plane was set to a constant, calculated through a 2-D mass balance as described earlier. The 200-mm-long inlet pipe was assumed to be sufficiently long to develop a standard seventh root velocity profile typical of turbulent pipe flow.[17] The constant values of K and ε set across the inlet plane according to this assumption were similar to those found at the outlet plane (Table II). Wall functions were used as boundary conditions on all solid surfaces, and the symmetry plane and outlet boundaries were the same as discussed previously for the full caster model. The solution strategy was also the same as for the mold simulation, and convergence was usually reached in only 8 to 10 iterations. A typical run required 90 minutes CPU time on the Ridge 32 or less than one minute on the CRAY X/MP.

B. *Nozzle Model Results*

Tables II and III show the calculated results for the range of nozzle angles and casting speeds considered in this study, using the properties and standard conditions given in Table I. Figure 2 shows the flow patterns calculated at various nominal nozzle angles, using water properties and a 1 m/min casting speed. Notice that the fluid always flows out through the bottom half of the nozzle outlet port. Every plot shows some recirculating flow near the top half, where steel actually flows into

Table II. Nozzle Model Outlet Results for Different Nominal Nozzle Angles

Nominal Angle		Water	Steel
30 deg up	angle	9.8 deg	10.5 deg
	average K (m^2/s^2)	0.0807	0.0685
	average ε (m^2/s^3)	0.8971	0.7951
	average normal inlet velocity (m/s)	0.8574	0.8544
15 deg up	angle	14.8 deg	15.4 deg
	average K	0.0694	0.0605
	average ε	0.6646	0.6023
	average normal inlet velocity	0.8599	0.8035
0 deg	angle	21.0 deg	21.5 deg
	average K	0.0571	0.0514
	average ε	0.4525	0.4414
	average normal inlet velocity	0.7939	0.7934
15 deg down	angle	27.7 deg	28.3 deg
	average K	0.0574	0.0502
	average ε	0.4414	0.3935
	average normal inlet velocity	0.7417	0.7434
30 deg down	angle	33.9 deg	34.0 deg
	average K	0.0522	0.0446
	average ε	0.3766	0.3394
	average normal inlet velocity	0.6837	0.7281

the nozzle. This behavior was also observed consistently in the Inland water model, even though it is difficult to discern in the photographs. Because of the flow across the top of the nozzle exit ports is very slow and into the nozzle, the nominal angle of the top edge of the exit port would not be expected to affect the flow. In fact, a water modeling study that varied the upper and lower nominal angles independently has confirmed that the nominal angle of the upper edge of the outlet port has no effect on the angle of the jet.[4]

Weighted average values for the effective outlet angle, K, ε, and average outlet velocity were calculated over the nozzle exit based on the magnitude of the positive outwardly flowing velocities. These values were then used as inlet conditions for the model simulations using the full mold.

V. PHYSICAL WATER MODELING EXPERIMENTS

Flow visualization experiments were performed on a full-scale, 0.686-m (54-in.)-wide by 0.229-m (9-in.)-thick physical water model under a variety of casting conditions. This "water caster" is a transparent plastic representation of an actual slab caster used at Inland Steel, except that its length is only 1.118 m (44 inches). The outlet of the model has 3 rows of small holes spaced 2 inches apart along the bottom piece of plastic, to allow removal of water at a rate equal to the casting speed.

Figure 3 presents a photograph of the overall flow pattern developed inside the physical water model, using a real steel slab-casting nozzle angled 25 deg downward, cast at 1 m/min, and visualized with 5 pct air bubble injection. Figure 4 illustrates the typical features of the flow pattern in a symmetric half of the physical water model, developed after viewing video tapes of the flow, visualized in three different ways: (1) dye injection into the flow in several locations, (2) the addition of small, plastic particles with a density close to that of water, and (3) air bubble injection through the nozzle. This schematic and photograph both show how the jet spreads outward until it impinges against the narrow face. It then spreads in all directions, resulting in a 3-D flow pattern locally. However, the bulk of the flow splits either downward or upward to the meniscus to flow back along the free surface to the nozzle. The result is four slowly recirculating zones, all of which eventually bring fluid back to the nozzle.

Figure 5 shows dye injection near the nozzle jet, its diffusion into the turbulent eddies, and formation of a plume. The plume drifts downward until it intersects the nozzle jet, then bends sharply with the jet toward the narrow face wall. The low bending point of the plume indicates that little flow exits the top half of the nozzle, as predicted by the nozzle model. This figure also shows the intense turbulence and swirling of the jet.

The dye plume suggests that, for a nominal 15 deg downward angled nozzle, the angle of the nozzle jet is

Table III. Nozzle Model Outlet Results for Different Casting Speeds (Steel)

Casting Speed	0.5 m/min	0.75 m/min	1.0 m/min	1.5 m/min	2.0 m/min
Inlet angle	27.5 deg	27.9 deg	28.3 deg	28.5 deg	28.6 deg
Average K (m^2/s^2)	0.0212	0.0355	0.0502	0.0850	0.1282
Average ε (m^2/s^3)	0.0839	0.2170	0.3935	1.0920	2.2932
Average normal inlet velocity (m/s)	0.3732	0.5600	0.7434	1.1092	1.4719

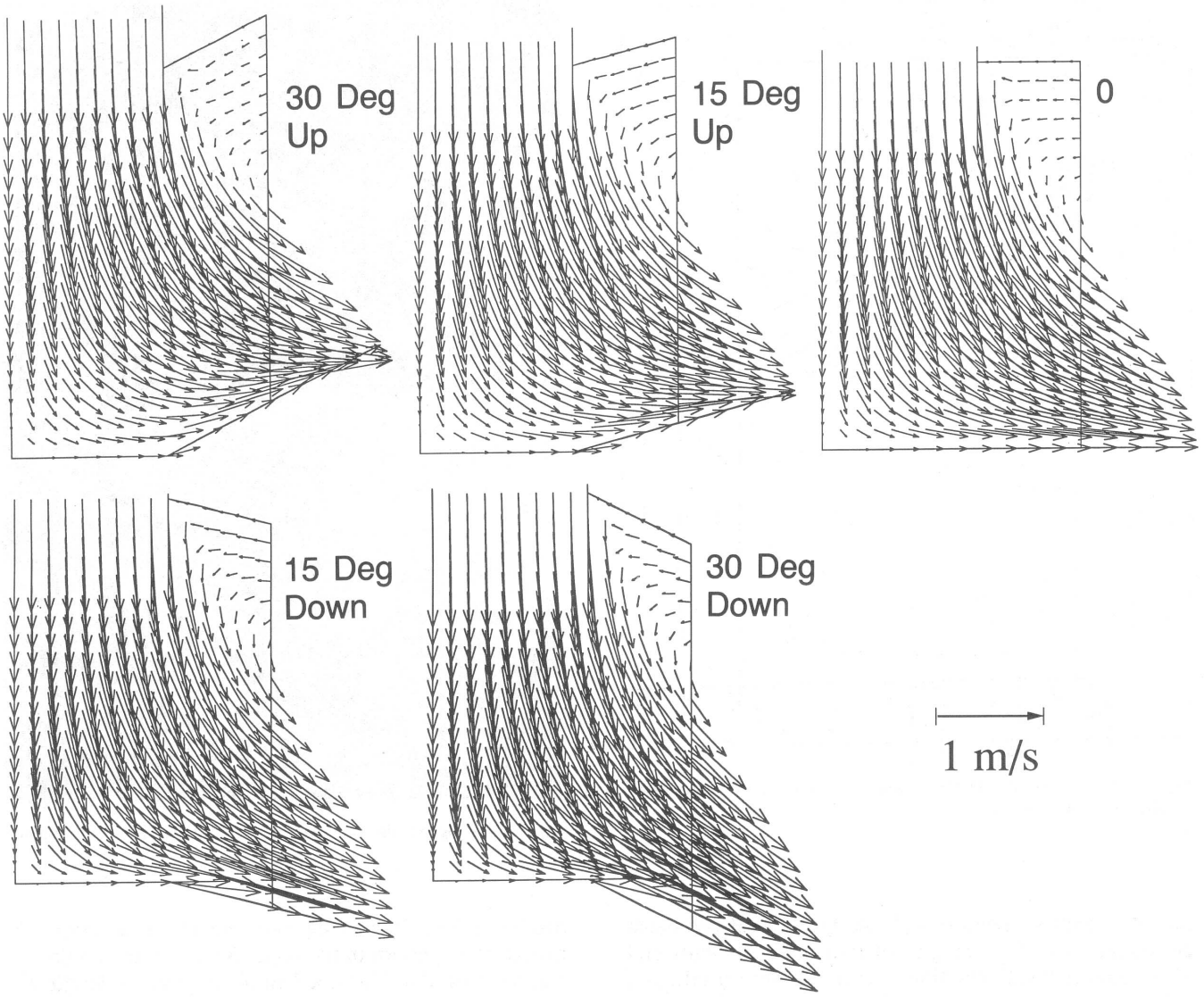

Fig. 2—Nozzle model results for five different nominal outlet angles of the nozzle ports.

about 30 deg downward, which agrees with the angle extracted from plastic particle injection. The angle obtained from air bubble injection, shown in Figure 6, was slightly larger (about 35 deg). The center of the impingement zone of the inlet jet on the narrow face wall of the physical water model was determined from observation to be about 100 mm above the bottom of the mold.

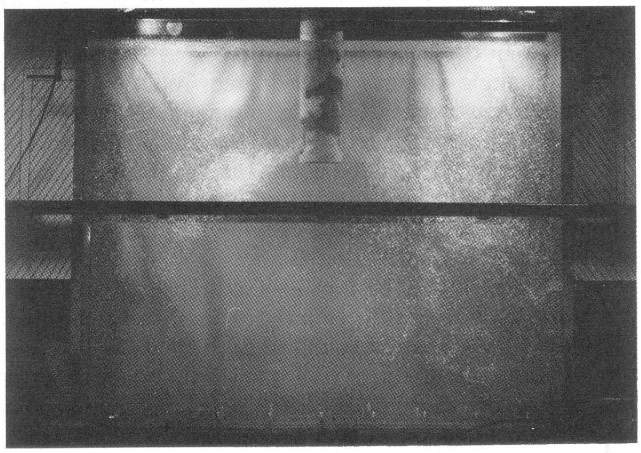

Fig. 3—Photograph of physical water model with 25 deg downward nozzle, visualized with air bubble injection.

It should also be noted from these photographs that a great deal of variability exists in flow in the physical model. Slight misalignment causes asymmetrical flow from opposite sides of the nozzle. This results in greatly varying turbulence and jet angles that can differ by as much as 5 deg. The flow was also seen to vary over time and depends on many other variables than the ones focused upon in this study. These include the amount and location of gas entrainment in the stream, the submergence depth, the mold width, and even the tundish level.

VI. MATHEMATICAL MODEL VERIFICATION AND RESULTS

To test the accuracy of model predictions of fluid velocity, fluid flow simulations of the physical water model at Inland Steel were performed. The results were then compared with the experimental findings using the water

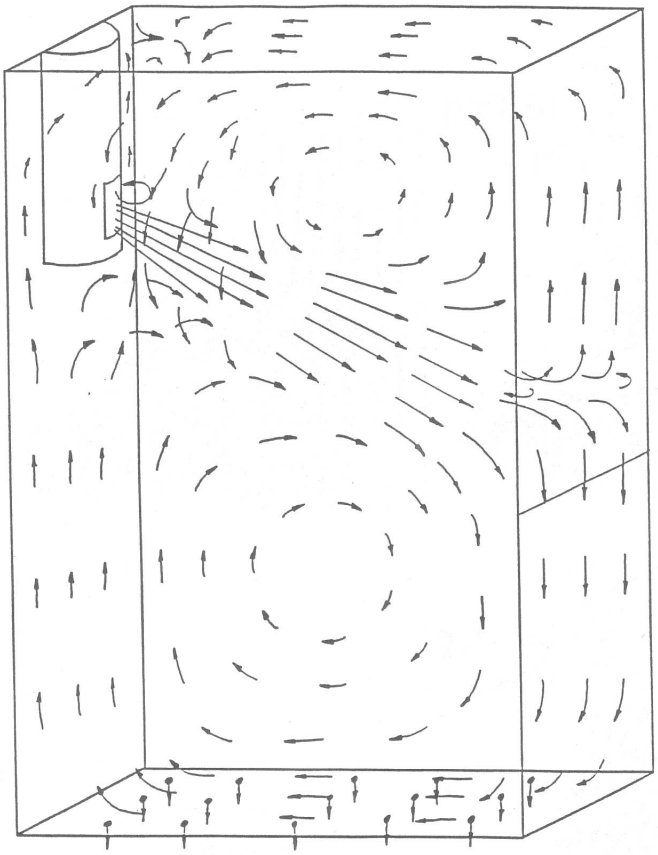

Fig. 4—Schematic of 3-D flow pattern observed in symmetric half of physical water model.

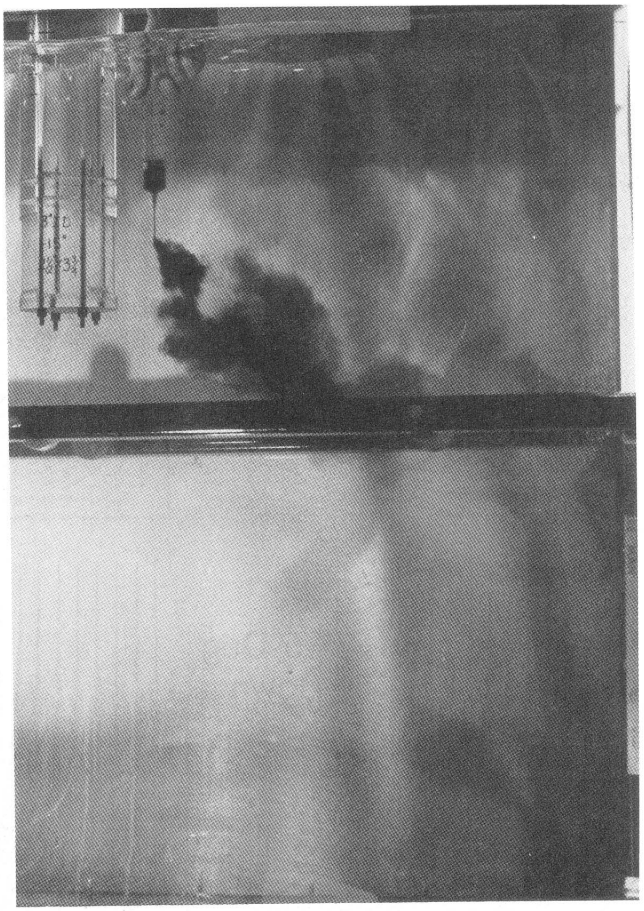

Fig. 5—Photograph showing dye injection just above the nozzle outlet.

model. Standard conditions (Table I) and a refined mesh consisting of a 40 × 75 grid of four-node elements and 75 two-node "wall function" elements were used. The velocity boundary conditions had to be modified at the outlet to account for the bottom of the physical model. This was accomplished by constraining the normal (vertical) velocity to zero at every second node along the bottom outlet boundary, which coincided conveniently with holes in the physical model.

A. *Effect of Outlet Boundary Condition and Model Domain Length*

Figure 7 shows that the velocity field inside the physical water model at Inland Steel is affected by its bottom. In an effort to determine how long a physical water model must be to prevent forced recirculation from hampering the accurate prediction of the fluid flow in the mold region, the effect of model domain length was investigated.

Simulations were performed using model domain lengths varying from 1.12 to 6.0 m, and the outlet normal (vertical) velocity was left unconstrained. These results showed that recirculation extends to substantial depths below the mold in the caster, and the flow does not become quiescent until almost 6 m deep in the strand. Flow leaving the 6-m model was almost uniform at the casting speed. Although flow through the outlet of the 3-m model was not uniform, it was almost identical to the velocity profile at 3 m deep in the 6-m model. In addition, the overall flow pattern in the upper 3 m of both simulations was very similar. Thus, a 3-m model domain length and unconstrained outlet velocity seemed the most appropriate choice for the remaining simulations.

Figure 7 compares the calculated flow patterns in the 1.12-m fixed bottom water model with the upper part of an unconstrained 3-m model of a steel caster. Generally, the velocity fields produced by the two models are very similar, particularly in the upper regions near the jet. However, the bottom of the short water model forces the flow to recirculate prematurely. This produces higher velocities in the lower recirculation zone and bends the water jet angle upward a few degrees relative to that in the bottomless steel caster. The impingement point is unaffected. Although the bottom does not appear to significantly affect flow in the upper zone, which is generally of greatest importance, the differences in the lower zone might affect the distribution of entrained particles in inclusion particle distribution studies.

A physical model of 2 m in depth appears to be sufficiently long to prevent interference of the bottom on the flow for the standard conditions in Table I. The minimum length required for accurate flow simulation using a physical model actually depends on the casting conditions and mold geometry. Greater widths, higher casting speeds, and steeper downward pointing nozzle angles would all require a longer physical model.

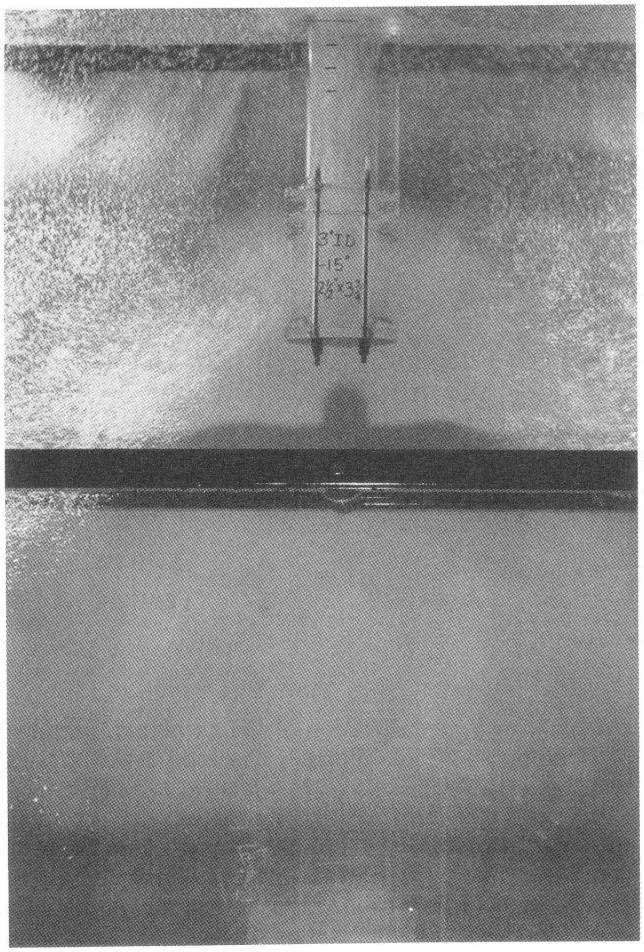

Fig. 6—Photograph of a 15 deg downward inlet nozzle in use in the water model.

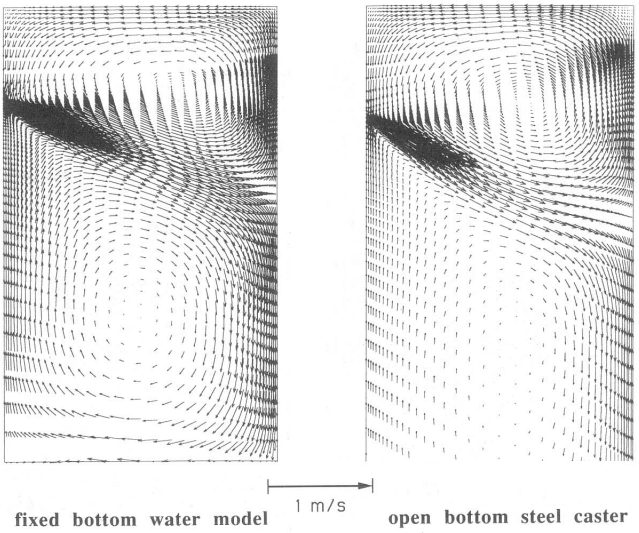

Fig. 7—Comparison of calculated velocities in the 1.12-m water model with fixed plastic bottom and the 3-m model with open bottom.

B. *Effect of Inlet Boundary Conditions*

The boundary conditions for K and ε at the inlet to the caster and the inlet velocity have been found to be very influential on both the results and numerical convergence.[16] Thus, the effect of different boundary conditions was explored by varying the values of K and ε used across the inlet plane of the caster model. The results are shown in Figure 8. Significant differences in jet angle can be seen with different boundary conditions. Increasing K appears to steepen jet angle, while increasing ε decreases angle. Recent experience has shown that these turbulence parameters also have an even greater influence on the temperature fields. Thus, it is crucial to find acceptable values for these parameters at the inlet.

An earlier method was employed to avoid this problem by setting the gradients of all variables, including K and ε, to zero across the inlet. Unfortunately, this proved to be very computationally expensive since the solution had poor stability and required incremental adjustment of material properties such as density and over 100 iterations before convergence was reached. This required roughly six times the execution time of the method presently used, although it produced similar flow results.

The present procedure fixes values across the inlet, which lets the model propagate the solution downstream. Flow in the caster interior is much less sensitive to values at the inlet of the nozzle pipe, since they are further removed upstream in the flow. To get these values, the nozzle model is run iteratively until K and ε values produced at the nozzle outlet plane (which is also the caster inlet plane) are similar to the nozzle inlet condition. Nozzle model runs using a variety of inlet boundary conditions, including profiles that varied across the diameter of the pipe, determined that the velocities, K, and ε at the outlet were quite insensitive to these inlet values, even when K and ε were varied by over an order of magnitude. This finding was expected; since the inlet pipe was sufficiently long to produce fully developed turbulent pipe flow, it could develop the corresponding K and ε values at the same time.

C. *Effect of Nozzle Port Angle*

To investigate the effect of the angle of the nozzle port edges on the overall flow pattern, the nozzle model was first run to determine the proper inlet boundary conditions, as discussed earlier and shown in Figure 2. It is particularly striking to note that the fluid momentum always produces downward flow from the nozzle, even when the nozzle edges are angled upward as steeply as 30 deg. Examining results from the caster simulations, the effective angle of the inlet jet was found to be greater (steeper downward) than the nominal angle of the nozzle port edges for the entire range of angles investigated. This effect is attributed to the downward momentum of the fluid. It was also observed in the physical water model and has been noted by other investigators, using both physical[2] and mathematical[10] models. The effect is quantified and presented in Table IV (using standard conditions), where the estimated jet angles observed in both the mathematical results and in the water model are compared.

The effect of varying nozzle angle affords an ideal opportunity to compare the mathematical model predictions with the physical water model observations. Figure 9

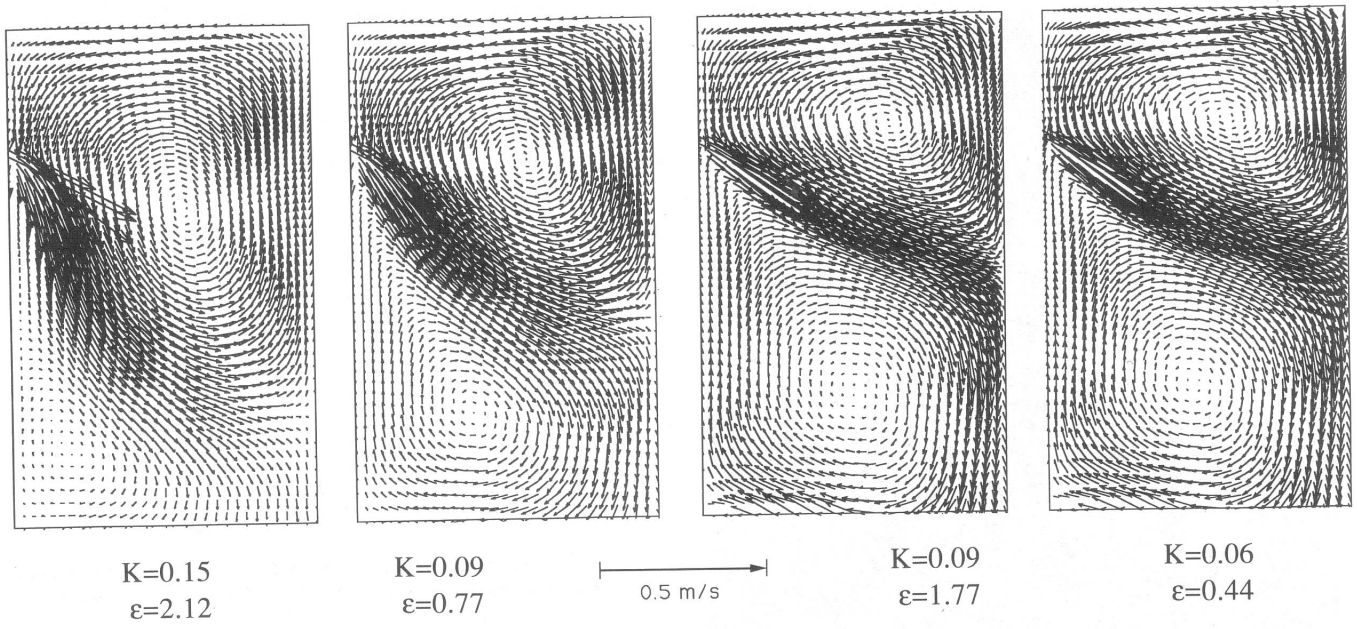

Fig. 8—Effect of K and ε inlet values on calculated velocities in the water model.

shows a photograph of the flow pattern in the water model resulting from a nominal 15 deg downward angled nozzle compared with the calculated streamlines for the same conditions (Table I) as Figure 7. The calculated results show general qualitative agreement with the overall flow pattern, shape, and direction of the jet plume, impingement point, and fluid velocities observed in the physical water model.

The angle of the fluid leaving the nozzle was found to control the flow in the mold interior. However, the spreading inlet jet is bent downward slightly by the recirculating bulk flow shortly after leaving the nozzle. The angle of the jet in the interior of the mold simulation was always found to be a few degrees steeper than the calculated average angle of the flow exiting the nozzle. In this example, the jet angle quickly steepened from its given inlet condition to almost 30 deg. This calculated jet angle is only slightly shallower than the approximately 35 deg downward angle observed in the water model.

Figure 10 shows the same comparison for a 15 deg upward angled nozzle. Both physical and mathematical

Table IV. Comparison of Estimated Jet Angles Observed in Mold Interior

Nominal Inlet Angle	Physical Model	Mathematical Model
30 deg up	—	15 deg down
15 deg up	20 deg down	20 deg down
0 deg (horizontal)	—	25 deg down
15 deg down	35 deg down	30 deg down
25 deg down	40 deg down	—
30 deg down	—	35 deg down

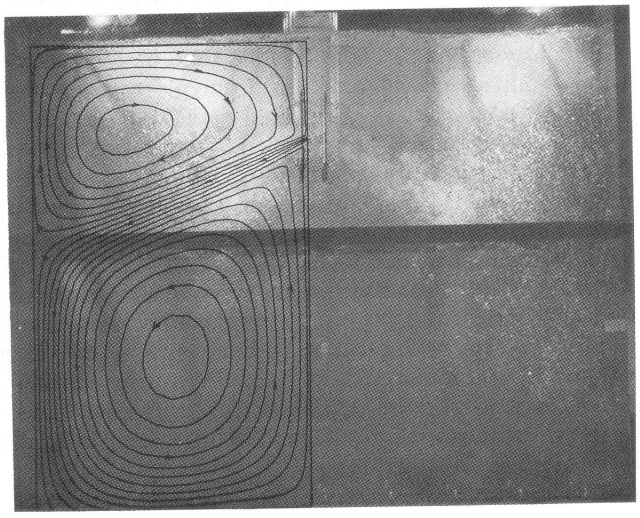

Fig. 9—Comparison of calculated and measured flow patterns in water model using 15 deg downward angled nozzles.

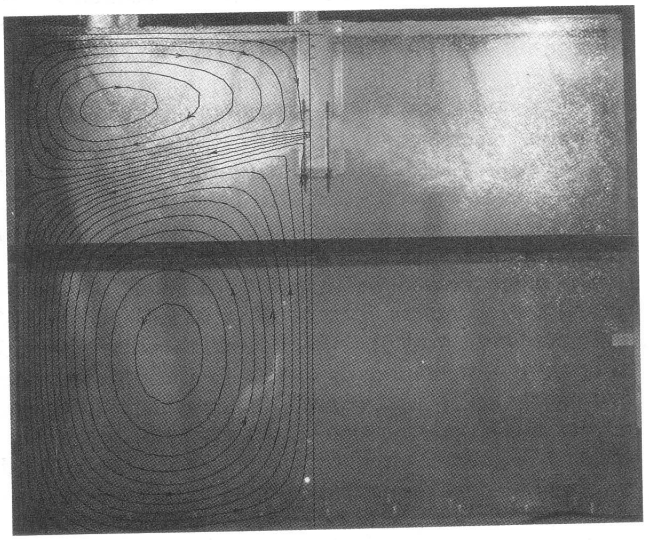

Fig. 10—Comparison of calculated and measured flow patterns in water model using 15 deg upward angled nozzles.

models exhibit a jet in the mold angled at roughly 20 deg downward. Ferretti *et al.*[2] observed that the jet from an upward facing nozzle fans more quickly and is accompanied by more turbulence and a major change in flow pattern, compared with the downward angled nozzle jets. Increased turbulence can also be seen in Figure 10, but there is no qualitative change in flow pattern.

As the nominal port angle is lowered, the effective jet angle increases, and the impingement point migrates down the narrow face wall. The magnitude of this expected result is fairly small, as seen in Figure 11. At the same time, the velocities below the impingement zone tend to increase slightly near the wall for large effective inlet angles. This latter effect could increase the probability of shell erosion over a distance of approximately 100 cm below the mold.

Table IV shows that the model calculations match the physical model observations of jet angle very well. The only deviation is a slight underprediction of the jet angle at steep downward port angles, but this is more likely due to interference from the bottom of the physical model. The agreement obtained is significantly better near the nozzle than that reported by Robertson *et al.*,[3] due to the influence of the nozzle model in the present simulation. This generates confidence that the 2-D model is capable of making reasonable flow predictions in an actual continuous caster.

D. *Effect of Casting Speed*

In addition to the standard casting speed of 1 m/min, the models were used to determine the effect of varying casting speed from 0.5 to 2.0 m/min. Higher casting speeds are of particular interest as the demand for increased productivity drives casters to increase their steel throughput. First, the nozzle model was used to find the inlet boundary conditions for runs at five casting speeds, using a nominal inlet angle of 15 deg down. These conditions produced the velocities shown in Figure 12. To allow qualitative comparison of the flow patterns generated with different casting speeds, the lengths of the velocity vectors in this figure have been scaled with respect to the maxima of each solution. Thus, vectors of the same length on the different plots do not correspond to the same speed.

In general, there is very little difference between the plots. This agrees with previous experience using physical models; that is, once a fully turbulent flow field has been developed, the actual flow rates do not greatly affect the flow pattern itself.[18] Observations of the Inland water model confirm this result. Jet angles were found to remain within 2 deg with increasing casting speed from 1.0 to 1.5 m/min. This is less than the variation between the two "symmetrical" jets, which have been seen to differ by as much as 5 deg in the water model.

Figure 13 shows that velocities through the outlet of the computational domain, 3 m below the meniscus, differ greatly with casting speed. Although the relative velocities remain the same, much higher velocities are predicted along the wall at higher casting speeds, which tend to force recirculation of fluid deeper into the caster. This will affect convective heat transfer to the solidifying shell, both deep in the caster, where fluid flow-enhanced heat flow will extend deeper into the caster, and near the critical meniscus-wall interface. Most importantly, the maximum heat flux occurring beneath the point of

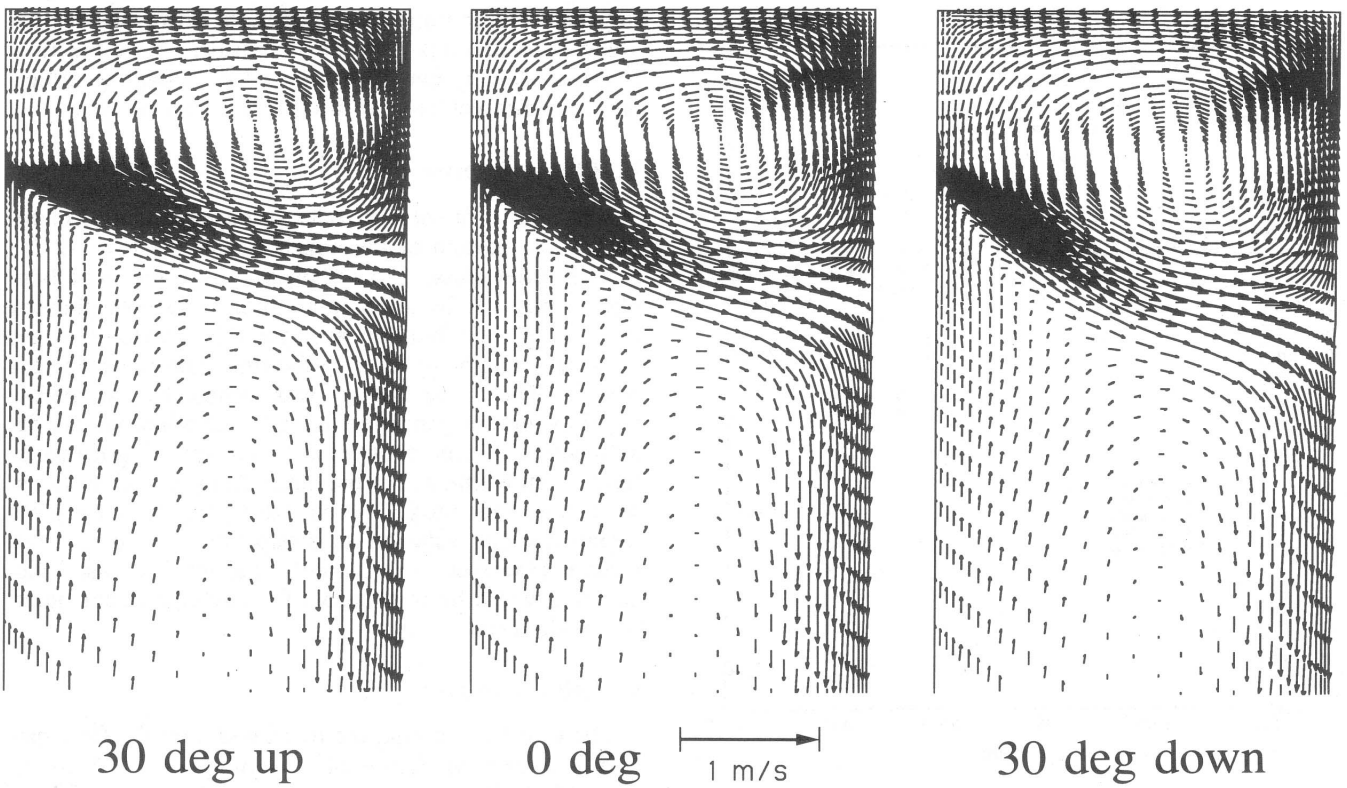

Fig. 11—Effect of nominal nozzle angle on caster velocity solution (standard conditions).

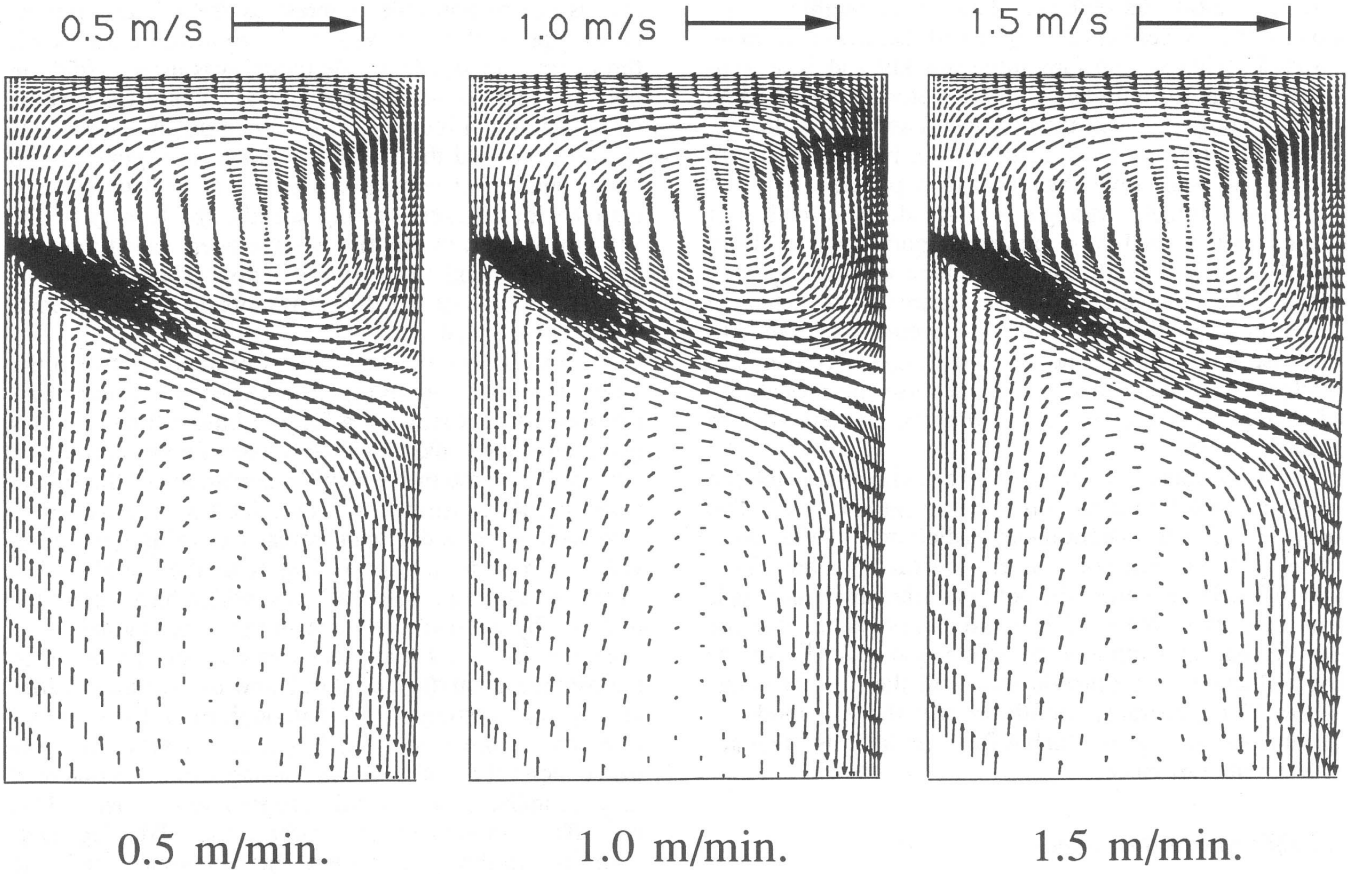

Fig. 12—Effect of casting speed on caster velocity solution (standard conditions).

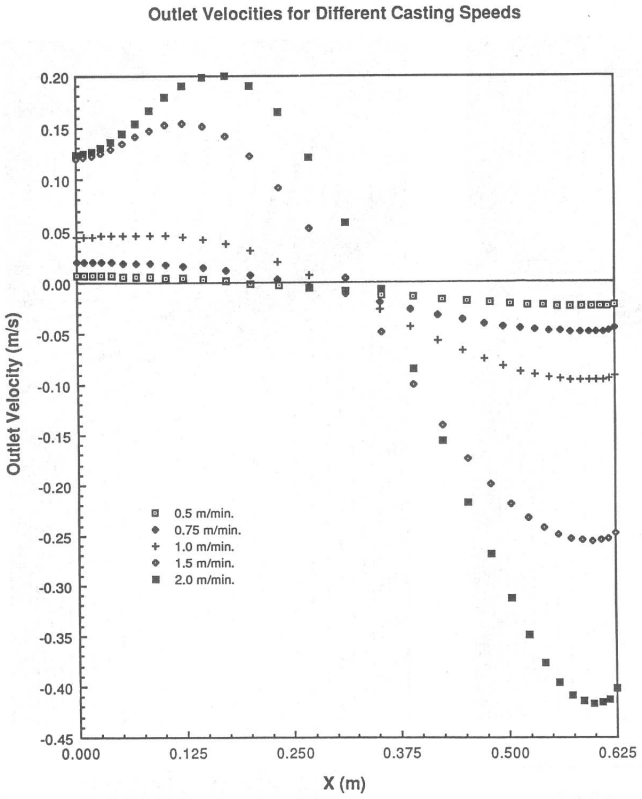

Fig. 13—Effect of casting speed on velocity profile across caster width (3.0 m below meniscus).

impingement should be greatly increased at higher casting speeds. It is important to caution, however, that the velocity predictions deep in the caster, where the flow is much slower, could be altered by buoyancy effects and have not yet been verified with experiments.

E. *Effect of Nozzle Well*

Industrial bifurcated nozzles often have a well or recess at the bottom of the nozzle below the level of the nozzle outlet ports. This is believed by some to be beneficial, possibly by trapping alumina inclusions (thereby preventing their buildup and possible blocking of the nozzle) or maybe by altering the flow pattern exiting the nozzle. The latter theory was tested by comparing the flow pattern generated using the standard nozzle design with a 20-mm recessed well. The resulting flow patterns, both within and at the outlet from the two nozzles, were almost identical. The only difference was a slightly higher average value of ε, dissipation, in the recessed nozzle. However, it is unlikely that this increased dissipation would be responsible for any significant quieting of the flow.

F. *Effect of Mold Width*

The effect of varying the mold width on the flow pattern is shown in Figure 14, assuming standard conditions (Table I) including a constant casting speed of 1 m/min. The model predicts that the steel jet will impinge

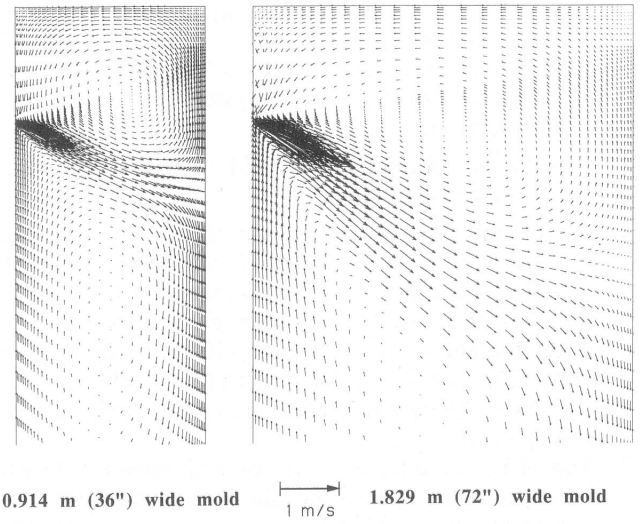

Fig. 14—Effect of mold width on caster velocity solution (standard conditions).

at successively lower points on the narrow face shell wall as the mold width increases and the jet travels further. Specifically, the impingement point lowers from 175 mm above the mold exit to 30 mm below the mold exit, as the width increases from 0.91 m (36 in.) to 1.83 m (72 in.). Since heat extraction by the sprays just below the mold on the narrow face is generally much less than in the mold, this implies an increased danger of a breakout for the wider slabs under these conditions.

The model also predicts, as observed in water models,[5] that the jet leaving the nozzle broadens more greatly in wider molds. Although the boundary of the jet is difficult to define sharply due to the continuous nature of the model calculations, the angle formed by the expanding cone appears to increase from about 15 deg for the thin 0.91-m slab to 25 deg for the wide 1.83-m slab, which is again in rough agreement with experimental observations.[5] For the wide mold (1.83 m), the width of the jet exceeds the thickness of the mold (0.203 m) by the time it reaches the narrow face, indicating that impingement on the corners of the wide faces will occur first. This will have the important consequence of promoting shell thinning in the critical off-corner region of the wide faces.

It should be noted that when significant air bubble injection is used (representing argon in the steel caster), the effect of the resulting lower density of the steel jet on the flow pattern becomes increasingly important away from the nozzle. This effect is most pronounced for wider slabs, where the increased distance traveled by the jet allows more time for its increased buoyancy to lift it toward the surface. Other research with water models[5] has observed that this effect can become so significant that the entire recirculation pattern changes for wider slabs. The jet can penetrate the top surface, resulting in flow near the top side corner heading *toward* the meniscus and *down* the narrow face. The model will not be able to simulate this effect until two-phase flow is included in the formulation.

The maximum velocities leaving the nozzle of wider slabs are much higher (0.80 m/s for the 0.914-m slab compared with 1.36 m/s for the 1.828-m-wide slab), since the casting speed was held constant at 1 m/min for all simulations. This would tend to deliver more heat to the narrow face and create shell-thinning problems for wide slabs. In addition, since heat extraction by the sprays just below the mold on the narrow face is generally much less than in the mold, the lower impingement point predicted on wide slabs would further increase the danger of a breakout for wider slabs under these conditions. However, the jet also has further to travel across the wider slab and, consequently, more time to broaden and diffuse heat. It is therefore difficult to conclude what the effect of mold width is on heat input to the narrow face without heat transfer calculations.

G. *Effect of Nozzle Submergence Depth*

Figure 15 shows the effect of changing the depth of submergence of the nozzle in the mold. The overall flow pattern remains almost exactly the same for nozzle outlet ports centered from 0.165 to 0.365 m below the meniscus. The change in impingement point of the jet on the narrow face corresponds almost exactly to the change in submergence.

It is interesting to note that observations of the water model showed a significant increase in surface turbulence with decreasing submergence depth. The model calculations do not indicate much evidence for this, except for a slight (5 pct) increase in velocities across the top surface for the shallower nozzle. The discrepancy might simply indicate a deficiency in the model in predicting surface turbulence, without special modeling of the top free surface effects. Alternatively, these results can be explained if most surface turbulence is associated with argon bubble injection and its effect on the buoyancy of the jet. Thus, the model predicts that if the jet was able to remain entirely below the surface until impingement with the narrow face (which is possible when there is no argon injection), then a similar low amount of surface turbulence would result.

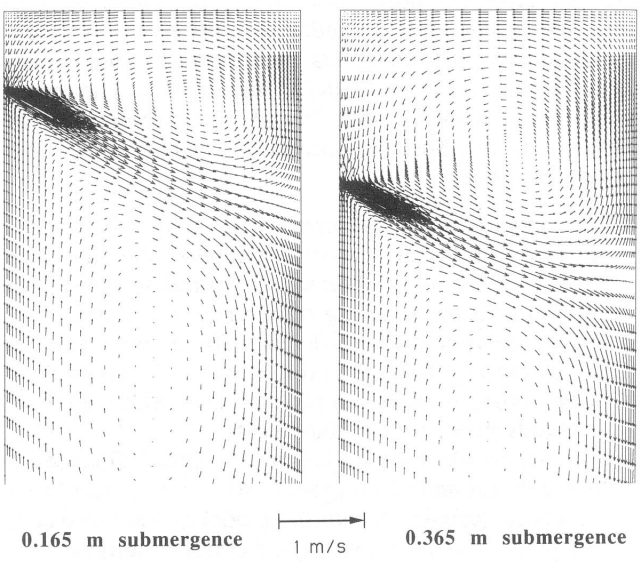

Fig. 15—Effect of nozzle submergence depth on caster velocity solution (standard conditions).

VII. COMPARISON BETWEEN STEEL AND WATER MODEL PREDICTIONS

Having compared the mathematical model to physical observations with some success, it was then applied to solve the steel continuous-casting problem. The velocity field calculated by the model for the standard conditions for steel from Table I generally resembles the flow patterns obtained in water model simulations, as seen in Figure 7. This was expected, owing to the large amount of successful experience using physical water models to predict flow in turbulent systems involving molten steel. The kinematic viscosity, μ/ρ, which is known to govern Reynolds number similarity and hence the flow pattern to a great extent, is about 0.95 for water and 0.78 for steel. This 18 pct difference was found to have very little effect on the flow pattern, as can be seen by comparing the water and steel nozzle outlet results in Tables II and III. Of much greater importance is the bottom required in the physical model, as discussed earlier.

A powerful feature of the analysis on the steel caster is the ability to input the velocity results into a subsequent uncoupled heat transfer model, which calculates the steady-state temperature distribution and heat flux input to steel shell solidifying against the narrow face mold, including the important areas near the meniscus and the jet impingement point. Eventually, these heat fluxes will be input, in turn, to a solidification model to calculate simultaneously, temperature, shrinkage, and stress development within the solidifying shell. The ability to couple together separate fluid flow and solidification models is desirable for the accurate prediction and understanding of shell growth and concurrent defect formation in an actual caster.

VIII. SUMMARY AND CONCLUSIONS

A mathematical modeling procedure has been successfully developed and applied to simulate turbulent fluid flow in the mold region of a continuous slab caster. The model is based on the K-ε turbulence equations and includes a separate model of the submerged, bifurcated inlet nozzle to provide inlet boundary conditions for the larger caster model. The model has been used to simulate flow inside a physical water model at Inland Steel. The results compare reasonably with visual observations of the physical model. Specific conclusions regarding the modeling procedure are:

1. The model results are sensitive to values of velocity, K, and ε at the inlet, so the simulation should extend as far upstream as necessary to simulate the proper flow conditions entering the domain of interest.
2. Better computational efficiency (by a wide margin) is achieved by fixing K and ε values at the inlet (rather than fixing their gradients to zero), although both methods produced similar results.
3. The Reynolds number has a profound influence on the solution and convergence, so it is essential to incorporate turbulence into the model and achieve convergence for the proper high Reynolds number.
4. If sufficient care is taken, mathematical models are capable of reproducing the flow phenomena observed in a turbulent, metallurgical system, such as a continuous slab-casting mold. Furthermore, a 2-D model can produce adequate results if the essential flow characteristics of the physical system are found in the simulated plane.

The model has correctly predicted several experimentally observed phenomena:

1. The overall flow pattern is reproduced by the model, including the angle of the fluid jet, the recirculation zones, and the point of impingement on the narrow face, under a variety of operating conditions.
2. A recirculation zone is found within the upper part of the inlet nozzle, which reduces the effective nozzle opening width by roughly half, increasing both velocity and turbulence.
3. The effective inlet angle is greater (steeper downward) than the nominal nozzle angle due to momentum of the liquid. In fact, use of an upward pointing nozzle port as steep as 30 deg still results in slightly downward flow from the nozzle.
4. The general recirculation pattern in the upper mold is influenced very little by increasing casting speed.
5. Flow in a full-scale physical water model is generally similar to that in an operating caster.

The model also makes other interesting predictions regarding the flow behavior:

1. The bottom of the physical water model interferes with the recirculation pattern. This problem is alleviated if the model is at least 3-m long.
2. The presence of a recess or well in the nozzle has little effect on the flow velocity exiting the ports.
3. The turbulence parameters, K, and ε at the inlet increase significantly with increasing casting speed, but the effective inlet angle increases (steepens) almost negligibly.
4. The velocities at the outlet of the domain vary considerably with increasing casting speed. Much more steel flows down near the narrow face at exit from the mold at high casting speeds, while the outlet velocity profile is almost flat at low speeds.

The present mathematical model is deficient for some applications, due to its 2-D nature, neglect of buoyancy effects, difficulties predicting surface turbulence effects, and lack of heat transfer prediction. However, even before making these improvements, the model is a powerful tool that is available for qualitative investigation of fluid flow within continuous slab-casting molds.

APPENDIX

Model equations

This 2-D, steady-state, incompressible, fluid-flow problem must solve for two unknown velocity distributions, v_x, and v_y, and the pressure distribution, p, which are governed by the continuity equation and two momentum equations:

Continuity Equation

$$\frac{\partial v_x}{\partial x} + \frac{\partial v_y}{\partial y} = 0 \qquad [1]$$

Momentum Equations

$$\rho\left(v_x\frac{\partial v_x}{\partial x}+v_y\frac{\partial v_x}{\partial y}\right)=-\frac{\partial p}{\partial x}+\rho f_x+2\frac{\partial}{\partial x}\mu_{\text{eff}}\frac{\partial v_x}{\partial x}+\frac{\partial}{\partial y}\mu_{\text{eff}}\left(\frac{\partial v_x}{\partial y}+\frac{\partial v_y}{\partial x}\right) \quad [2]$$

$$\rho\left(v_x\frac{\partial v_y}{\partial x}+v_y\frac{\partial v_y}{\partial y}\right)=-\frac{\partial p}{\partial y}+\rho f_y+2\frac{\partial}{\partial y}\mu_{\text{eff}}\frac{\partial v_y}{\partial y}+\frac{\partial}{\partial x}\mu_{\text{eff}}\left(\frac{\partial v_x}{\partial y}+\frac{\partial v_y}{\partial x}\right) \quad [3]$$

The effective viscosity, μ_{eff}, needed in Eqs. [2] and [3] is defined as the sum of laminar (or molecular) and turbulent (or eddy) viscosity components:

$$\mu_{\text{eff}}=\mu_{\text{lam}}+\mu_t \quad [4]$$

The turbulent component, μ_t, is then found from the K-ε model parameters, K and ε, by

$$\mu_t=C_\mu\rho\frac{K^2}{\varepsilon} \quad [5]$$

These two parameters are, in turn, found by solving two additional transport equations for the turbulent kinetic energy, K, and its rate of dissipation, ε, as given below:

Turbulence Equations

$$\rho\left(v_x\frac{\partial K}{\partial x}+v_y\frac{\partial K}{\partial y}\right)=\frac{\partial}{\partial x}\left(\frac{\mu_t}{\sigma_K}\frac{\partial K}{\partial x}\right)+\frac{\partial}{\partial y}\left(\frac{\mu_t}{\sigma_K}\frac{\partial K}{\partial y}\right)+\rho G_K-\rho\varepsilon \quad [6]$$

$$\rho\left(v_x\frac{\partial \varepsilon}{\partial x}+v_y\frac{\partial \varepsilon}{\partial y}\right)=\frac{\partial}{\partial x}\left(\frac{\mu_t}{\sigma_\varepsilon}\frac{\partial \varepsilon}{\partial x}\right)+\frac{\partial}{\partial y}\left(\frac{\mu_t}{\sigma_\varepsilon}\frac{\partial \varepsilon}{\partial y}\right)+C_1\frac{\varepsilon}{K}\rho G_K-C_2\frac{\varepsilon^2}{K} \quad [7]$$

where G_K, the generation of K, $=(\mu_t/\rho)\{2(\partial v_x/\partial x)^2+2(\partial v_y/\partial y)^2+[(\partial v_y/\partial x)+(\partial v_x/\partial y)]^2\}$. These equations involve five empirical constants, which are given standard values[14,15] as follows:

$$C_1=1.44; \quad C_2=1.92; \quad C_\mu=0.09;$$
$$\sigma_K=1.0; \quad \sigma_\varepsilon=1.3 \quad [8]$$

Wall function boundary conditions

The governing equations are subject to a boundary condition on every edge of the computational domain for v_x, v_y, K, and ε, or their gradients. These include wall functions imposed on those edges adjacent to solid surfaces. The best results were obtained when the following set of conditions were employed along the vertical boundary:

v_x, normal velocity $= 0^*$ [9]

*When the wall is tapered to account for the presence of the growing shell, the normal velocity must account for steel leaving the computational domain by moving across the solidifying shell interface: v_x = casting speed * final shell thickness/model domain length.

$$\frac{\partial v_y}{\partial x}\text{, tangential velocity gradient} = \frac{\rho}{\mu_t}\left(\frac{\kappa v_y}{\ln\left(E\frac{\rho y_n C_\mu^{0.25}K^{0.5}}{\mu_{\text{lam}}}\right)}\right)^2\frac{v_y}{|v_y|} \quad [10]$$

$$\frac{\partial K}{\partial x}\text{, kinetic energy gradient} = 0 \quad [11]$$

$$\varepsilon\text{, dissipation} = \frac{C_\mu^{0.75}K^{1.5}}{\kappa y_n} \quad [12]$$

where the following additional constants are defined as

κ, von Karman constant, $= 0.41$;
E, wall roughness constant, $= 9.0$; and
y_n, distance the computational domain is offset from the wall, $= 0.01$ m.

ACKNOWLEDGMENTS

The authors wish to express thanks to Inland Steel Company, East Chicago, IN, ARMCO, Inc., Middletown, OH, and Bethlehem Steel, Bethlehem, PA, for their support of this research project. Additional thanks are extended to Inland Steel for the use of their physical water modeling facility, the provision of valuable data, and for the help and kind advice received from several Inland personnel, in particular, Ismael Saucedo, Yeou-H. Wang, and John Mudrovich. Acknowledgment is also given to the National Center for Supercomputing Applications at the University of Illinois for providing time on the CRAY X/MP 48. Finally, the authors are grateful to Fluid Dynamics International, Inc., Evanston, IL, and Vahe Haroutunian for help with the FIDAP program.

REFERENCES

1. H. Nakato, M. Ozawa, K. Kinoshita, Y. Habu, and T. Emi: *Trans. Iron Steel Inst. Jpn.*, 1984, vol. 24 (11), pp. 957-65.
2. A. Ferretti, M. Podrini, and G. Si Schino: *Steelmaking Proc.*, Iron and Steel Society, 1985, vol. 68, pp. 49-57.
3. T. Robertson, P. Moore, and J.F. Hawkins: *Ironmaking and Steelmaking*, 1986, vol. 13 (4), pp. 195-203.
4. N.A. McPherson: *Steelmaking Proc.*, Iron and Steel Society, 1985, vol. 68, pp. 13-25.
5. R. Sobolewski and D.J. Hurtuk: *2nd Process Technology Conf. Proc.*, 1982, vol. 2, pp. 160-65.
6. R.I.L. Guthrie: in *Mathematical Modelling of Materials Processing Operations*, TMS Conf. Proc., Palm Springs, CA, Nov. 29, 1987, J. Szekely, L.B. Hales, H. Henein, N. Jarrett, K. Rajamani, and I. Samarasekera, eds., pp. 447-82.
7. Y. Sahai: in *Mathematical Modelling of Materials Processing Operations*, TMS Conf. Proc., Palm Springs, CA, Nov. 29, 1987, J. Szekely, L.B. Hales, H. Henein, N. Jarrett, K. Rajamani, and I. Samarasekera, eds., pp. 431-45.
8. O.J. Ilegbusi and J. Szekely: in *Mathematical Modelling of Materials Processing Operations*, TMS Conf. Proc., Palm Springs, CA, Nov. 29, 1987, J. Szekely, L.B. Hales, H. Henein, N. Jarrett, K. Rajamani, and I. Samarasekera, eds., pp. 409-29.
9. F.G. Wilson, M.J. Heeson, A. Nicholson, and A.W.D. Hills: *Ironmaking and Steelmaking*, 1987, vol. 14 (6), pp. 296-309.
10. M. Yao, M. Ichimiya, K. Syozo, K. Suzuki, K. Sugiyama, and R. Mesaki: *Steelmaking Proc.*, Iron and Steel Society, 1985, vol. 68, pp. 27-34.

11. J. Kelly, K.P. Michalek, B.G. Thomas, and J.A. Dantzig: *Metall. Trans. A*, 1988, vol. 19A, pp. 2589-2601.
12. W. Rodi: *Turbulence Models and Their Application in Hydraulics—A State of the Art Review*, University of Karlsruhe, Karlsruhe, West Germany, 1980.
13. K. Spitzer, M. Dubke, and K. Schwertfeger: *Metall. Trans. B*, 1986, vol. 17B, p. 119.
14. M.S. Engelman: *FIDAP Theoretical Manual—Revision 4.0*, Fluid Dynamics International, Inc., Evanston, IL, 1986.
15. B.E. Launder and D.B. Spalding: *Mathematical Models of Turbulence*, Academic Press, London, 1972.
16. F.M. Najjar and B.G. Thomas: *Third FIDAP Users Conf.*, Fluid Dynamics International, Inc., Evanston, IL, Sept. 25, 1989.
17. L. Prandtl and O. Tietjens: *Applied Hydro- and Aeromechanics*, McGraw-Hill, New York, NY, 1934.
18. R.E. Johnstone and M.W. Thring: *Pilot Plants, Models and Scale-Up Methods in Chemical Engineering*, McGraw-Hill, New York, NY, 1957, p. 199.